

# Order Matters: On Parameter-Efficient Image-to-Video Probing for Recognizing Nearly Symmetric Actions

Thinesh Thiyakesan Ponbagavathi Alina Roitberg

Institute for Artificial Intelligence, University of Stuttgart, Germany

{thinesh.thiyakesan-ponbagavathi, alina.roitberg}@ki.uni-stuttgart.de

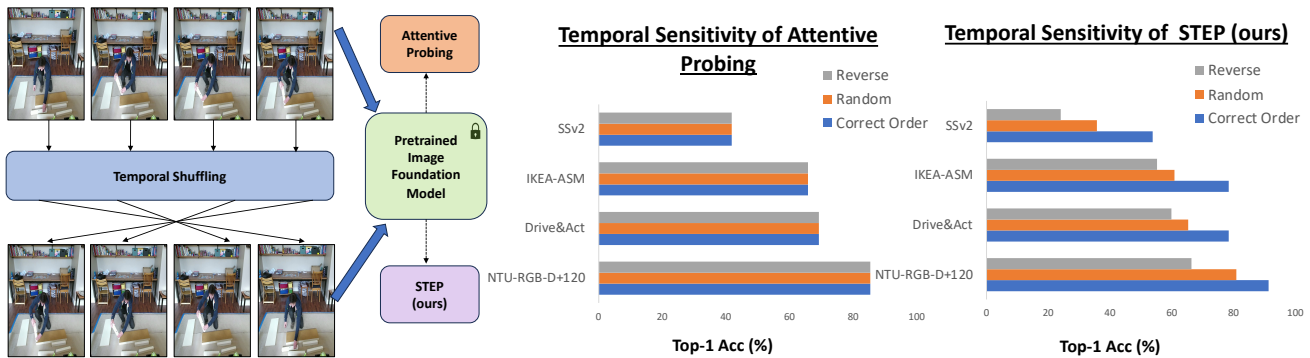


Figure 1. We showcase that attentive probing commonly used for parameter-efficient image-to-video transfer in activity recognition is invariant to temporal order of frames. Disrupting the frame order at test-time does not impact the outcome (left bar chart), making it hard to distinguish *nearly symmetric actions* – actions that are visually similar but differ in the sequence of events (e.g., *picking up* vs. *placing an object*). We propose Self-attentive Temporal Embedding Probing (STEP), which makes self-attentive probing sensitive to changes in frame order (right bar chart), leading to better recognition of fine-grained and nearly symmetric actions, with fewer learnable parameters.

## Abstract

We study parameter-efficient image-to-video probing for the unaddressed challenge of recognizing nearly symmetric actions – visually similar actions that unfold in opposite temporal order (e.g., opening vs. closing a bottle). Existing probing mechanisms for image-pretrained models, such as DinoV2 and CLIP, rely on attention mechanism for temporal modeling but are inherently permutation-invariant, leading to identical predictions regardless of frame order.

To address this, we introduce Self-attentive Temporal Embedding Probing (STEP), a simple yet effective approach designed to enforce temporal sensitivity in parameter-efficient image-to-video transfer. STEP enhances self-attentive probing with three key modifications: (1) a learnable frame-wise positional encoding, explicitly encoding temporal order; (2) a single global CLS token, for sequence coherence; and (3) a simplified attention mechanism to improve parameter efficiency. STEP outperforms existing image-to-video probing mechanisms by 3–15% across four activity recognition benchmarks with only 1/3 of the learn-

able parameters. On two datasets, it surpasses all published methods, including fully fine-tuned models. STEP shows a distinct advantage in recognizing nearly symmetric actions, surpassing other probing mechanisms by 9–19%, and parameter-heavier PEFT-based transfer methods by 5–15%. Code and models will be made publicly available.

## 1. Introduction

The transfer learning paradigm is rapidly shifting from “pre-train and finetune” to “pre-train then probe”, where foundation models keep their pre-trained representations, while lightweight probing layers handle task-specific adaptations. Several recent video activity recognition methods [1, 24, 29, 40, 46, 51, 55, 63, 66] rely on adapting image-pretrained foundation models, like CLIP [42] and DinoV2 [39], for video tasks, leveraging their generalization ability while avoiding the high cost of full fine-tuning.

Action recognition in video requires understanding both appearance and temporal dynamics. Probing-based meth-

ods [3, 9, 23, 39, 42, 52, 64, 65]—which modify only final-layer representations—lack explicit temporal modeling making them less effective for order-sensitive actions. PEFT (Parameter-Efficient Fine-Tuning) methods [21, 31, 40, 56, 59, 63] introduce lightweight temporal adaptations or learnable prompts, modifying earlier layers to enhance video transfer. While these methods perform well on large-scale datasets, they require more tunable parameters than probing and remain largely untested on smaller, fine-grained datasets.

Do probing and PEFT methods effectively capture action sequences and distinguish order-sensitive actions like *putting down vs. picking up*? For distinct actions like *clapping* and *waving* recognizing a few key frames is often sufficient. However, *nearly symmetric actions* like *opening a bottle vs. closing a bottle* share highly similar frames but differ in execution order, making implicit temporal modeling insufficient. Our experiments confirm that both probing and PEFT methods lead to confusion rates of up to 60%. Attentive probing [3, 25, 64], while effective for capturing appearance features, fails to model action order due to its permutation-invariant nature. As shown in Figure 1, reversing or shuffling frames does not impact recognition, confirming its limitation in temporal understanding. PEFT methods, though effective on large-scale datasets [16, 22], fail to generalize to smaller, fine-grained domain-specific datasets, where data efficiency and sequence understanding are critical. These findings underscore the need for a parameter-efficient approach that explicitly models temporal order, bridging the gap between probing and PEFT.

To address this limitation, we propose **Self-attentive Temporal Embedding Probing (STEP)**—a simple yet effective extension of self-attention probing that enhances temporal modeling while maintaining efficiency. Unlike PEFT methods, which modify earlier layers, STEP introduces explicit temporal modeling in the final probing layers through three key components: (1) a learnable frame-wise positional encoding reinforcing the video’s sequential nature, (2) a global CLS token shared across frames, encouraging temporal coherence in predictions and (3) a simplified attention block with no skip connections, layer norm or FF layers. While transformers encode position in early layers, probing methods remain permutation-invariant [3, 25, 64, 65]. STEP integrates temporal encoding in final layers, improving order sensitivity.

We benchmark STEP on four datasets: NTU-RGB+D 120 [30], IKEA-ASM [6], Drive&Act [38], and SSv2 [16], achieving accuracy gains of 3–15% on DinoV2 and 3–9% on CLIP over attentive probing using only 1/3 of the tunable parameters. STEP consistently outperforms probing across all benchmarks and surpasses PEFT methods in recognizing *nearly symmetric actions*. It achieves state-of-the-art results on IKEA-ASM and Drive&Act, which feature nu-

merous hand-centric and order-sensitive actions, improving recognition by 13.5% and 14.86%, respectively. On NTU-120, STEP outperforms PEFT on symmetric actions while maintaining high efficiency. Additionally, in the low-data setting of SSv2, STEP outperforms PEFT methods, highlighting its data efficiency, whereas PEFT methods struggle due to their reliance on large-scale training data.

To summarize our contributions: **1)** We analyze the limitations of both probing and PEFT methods in image-to-video transfer, showing that attentive probing is inherently invariant to frame permutations, while PEFT methods struggle in small, domain-specific datasets and nearly symmetric actions. **2)** To study this, we introduce and benchmark the concept of *nearly symmetric actions* – actions with similar frame content but opposite temporal order, and manually identify them at the category level in three datasets. **3)** We present STEP – a simple yet effective modification of self-attention probing, which integrates learnable frame-wise positional encodings, a frame-global CLS token and a simplified attention block to better model temporal order. **4)** We achieve state-of-the-art results on IKEA-ASM and Drive&Act, and surpass PEFT in *nearly symmetric actions* and low-data settings of SSv2, demonstrating superior data efficiency.

## 2. Related Work

**Probing Mechanisms in Foundation models.** Image foundation models like CLIP [42] and DinoV2 [39] excel in tasks such as classification [2, 18], segmentation [4, 20, 58], and retrieval [36, 43], often leveraging simple probing mechanisms on a frozen backbone. While tasks like image retrieval rely on non-parametric methods, (e.g., cosine similarity), classification often employs linear probing layers [9, 23, 52]. However, linear probes may lack expressiveness, as SimCLR [9] demonstrated that adding a non-linear projection head improves performance, particularly for models trained via masked modeling [17, 49]. More advanced probing strategies introduce attentive probing via cross-attention and learnable queries, as seen in CoCa [64] and Set Transformer [25], enabling better feature aggregation for diverse tasks [48, 49, 57, 64]. For image-to-video probing, common approaches include using a central frame [42], averaging frame-wise embeddings [3, 39, 54, 65], or concatenating frame-wise features with larger linear layers, as in DinoV2 [39]. Recent methods increasingly employ attentive probing [3, 64, 65] to capture temporal dependencies. However, these methods remain permutation-invariant [25], limiting their ability to recognize temporally complex actions. We address this by building on attentive probing with modifications that explicitly model temporal order.

**Temporal Modeling for Image-to-Video Transfer.** Temporal modeling in foundation models has evolved from frame-wise representations with learnable temporal en-

coders (e.g., X-CLIP, ActionCLIP [37, 54]) to spatiotemporal fusion via cross-attention [29]. Recent methods, such as STAN [32], BIKE [60], and ILA [50], further improve temporal reasoning by introducing auxiliary networks, bidirectional cross-modal alignment, and temporal alignment via learnable masks, respectively. Some methods make use of spatiotemporal patches, or tube embeddings, combined spatial and temporal information within ViT-based encoders, seen in models like VideoSwin [34], VideoMAE [49], CLIP4Clip [35], and InternVideo2 [57]. Despite their strong performance, these methods require full fine-tuning, making them computationally expensive.

To address this, Parameter-Efficient Fine-Tuning (PEFT) methods introduce lightweight adaptations for frozen models. ST-Adaptor [40] applies bottleneck layers for spatiotemporal transfer, while AIM [63] extends spatial attention to the temporal domain via adapters across spatial, temporal, and MLP layers. Vita-CLIP [59] employs multimodal prompts to capture temporal structure, whereas M2-CLIP [56] enhances temporal alignment using a TED-Adapter. While these methods perform well on large-scale datasets, their effectiveness on small, fine-grained datasets like IKEA-ASM and Drive&Act remains largely untested. In contrast, probing mechanisms adapt only the classification layer, offering lower parameter costs and working well for smaller datasets. However, existing probing methods are weaker than PEFT approaches in performance, limiting their effectiveness in video tasks. STEP bridges this gap by introducing a probing mechanism that is parameter-efficient yet explicitly models temporal order, improving performance on small, fine-grained datasets.

### 3. Self-attentive Temporal Embedding Probing for Recognizing Nearly Symmetric Actions

Our goal is to study temporal understanding in parameter-efficient image-to-video probing, focusing on the underexplored task of recognizing *nearly symmetric actions* – visually similar actions that differ in reversed temporal order (e.g., putting on vs. taking off a jacket).

We first examine the permutation invariance of self-attention and provide an overview of our backbone foundation models (Sec. 3.1). Then, we introduce Self-attentive Temporal Embedding Probing (STEP), which enhances temporal reasoning by integrating frame-wise temporal embeddings and a global CLS token (Sec. 3.2). Our hypothesis is that a stronger understanding of temporal order is particularly beneficial for recognizing nearly symmetric actions. To test this, we manually identify such action pairs in three public datasets and evaluate our method on both nearly symmetric and non-symmetric actions, as well as the full benchmarks. We detail these symmetric action splits in the experiments section (Sec. 4.1).

### 3.1. Preliminaries

**Self Attention and Permutation Invariance.** Self-attention [53] is the cornerstone of transformer architectures, computing relationships between all pairs of tokens in a sequence. For an input sequence  $x = \{x_1, x_2, \dots, x_n\}$  with  $n$  tokens, self-attention generates attention scores based on the dot product between token embeddings. Formally, tokens are projected into queries, keys, and values via learnable matrices ( $W_q, W_k, W_v$ ). The attention score for token  $x_i$  attending to  $x_j$  is computed as

$$\alpha_{ij} = \frac{\exp(q_i \cdot k_j / \sqrt{d})}{\sum_{j=1}^n \exp(q_i \cdot k_j / \sqrt{d})},$$

where  $d$  is the dimensionality of the query and key vectors, and  $\alpha_{ij}$  represents the attention weight of  $x_j$  for  $x_i$ . The output of the self-attention layer for token  $x_i$  is then  $z_i = \sum_{j=1}^n \alpha_{ij} v_j$ . As attention scores are computed independently of token order, self-attention is inherently permutation-invariant [25].

Consequently, attentive probing methods effectively aggregate frames but lack explicit temporal sensitivity. This is particularly advantageous when appearance cues dominate, but severely limits recognition for temporally nuanced or nearly symmetric actions, where the frame order is critical. Our experiments clearly illustrate this limitation, showing no accuracy changes when frame order is shuffled or reversed (Figure 1).

**Positional Encoding.** To address permutation invariance, transformers [53] use absolute positional encoding with sinusoidal functions. This encoding assigns each position a unique, fixed embedding based on sine and cosine functions, embedding sequence order without needing learnable parameters. Learnable absolute encodings [14] provide more flexibility by allowing the model to learn position-specific embeddings. Hybrid encoding combines both absolute and learnable embeddings, capturing both fixed positions and adaptable positional cues [45]. However, positional encodings are traditionally used at earlier layers and not during the probing stage. Current image-to-video probing frameworks tend to overlook the inclusion of any frame-wise positional information [3, 9, 23, 39, 42, 52].

### 3.2. Self-attentive Temporal Embedding Probing

We now introduce **STEP** - Self-attentive Temporal Embedding Probing (overview in Figure 2), which incorporates several simple but effective modifications to attention based probing for parameter-efficient image-to-video transfer. Consider a video sequence  $x = \{x_1, x_2, \dots, x_T\}$  processed frame-by-frame with a pre-trained and frozen image foundation model  $\theta_{\text{frame}}$ , resulting in frame representations,  $e_i, \theta_{\text{frame}} : \mathbf{x}_i \rightarrow e_i$ . Each frame is spatially split into  $n$  patches, forming a set of patch tokens  $e_i^{\text{patch}} = \{e_{i,1}, e_{i,2}, \dots, e_{i,n}\}$  and an additional CLS token  $e_i^{\text{CLS}}$  that provides a unified representation of the frame.

$$e_i = \{e_i^{\text{patch}}, e_i^{\text{CLS}}\} \quad (1)$$

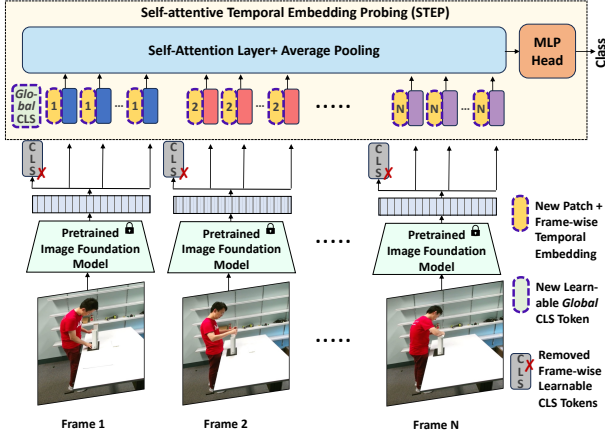


Figure 2. **Overview of Self-attentive Temporal Embedding Probing.** Each video frame is first independently processed by a frozen image model. We replace the frame-specific CLS token with learned patch-wise temporal encodings, while a newly added *frame-global* CLS token encourages temporal consistency in predictions, followed by a self-attention probing mechanism that keeps track of the temporal order through these modifications.

The goal of our STEP probing method, denoted as  $f$ , is then to link the frame-wise feature representations first into a sequence  $e = \{e_1, e_2, \dots, e_T\}$  then mapping this sequence to  $y$  – the target action label:  $f : e \rightarrow y$ .

Our method builds on the self-attention probing strategy for image-to-video transfer [25, 35] with two main modifications: (1) a global CLS token that aggregates information across frames instead of the frame-wise CLS tokens, and (2) frame-wise temporal embeddings to encode temporal order. These embeddings are then processed by a self-attention layer, average pooling, and a simplified classification head, as we consistently find that omitting certain common components of probing layers preserves action recognition accuracy while significantly reducing the parameter count.

**Learnable Global CLS Token.** STEP uses frame patch tokens and a **single learnable frame-global CLS** token,  $e_{global}^{CLS}$  to maintain a coherent global representation. This differs from the standard way [15, 39, 42] of using a separate CLS token for each frame. We explicitly discard frame-specific CLS tokens and employ a single learnable global CLS token that attends to all the patch tokens across frames:

$$e = \left\{ e_{global}^{CLS}, e_1^{patch}, \dots, e_T^{patch} \right\} \quad (2)$$

By attending to all patch tokens during self-attention, the global CLS token captures **global (sequence-level)** temporal dependencies. Meanwhile, **local (frame-level)** details are preserved by integrating frame-wise patch embeddings into the attention mechanism and classification layers, ensuring that STEP maintains fine-grained spatial information while modeling the overall temporal structure. This

design enhances temporal consistency by reducing redundancy across frames and consolidating the sequence into a single coherent representation, allowing the model to focus on key temporal transitions critical for action recognition.

**Injecting Temporal Embeddings in Self-attention Probing.**

To improve the temporal sensitivity of the existing probing mechanisms, we augment each frame representation  $e_i$  with a learned frame-specific temporal embedding, denoted by  $t_i$ . This results in a temporally enhanced frame embedding,  $\tilde{e}_i$ :  $\tilde{e}_i = e_i + t_i$ . However, since  $\tilde{e}_i$  consists of multiple spatial patch tokens (Eq. 2), temporal embedding  $t_i$  is applied to *each patch token* within the frame to ensure temporal information across all regions. Thus, for each patch token  $e_i^{patch}$  within frame  $e_i$ , the temporal embedding so added as  $\tilde{e}_i^{patch} = e_i^{patch} + t_i$ . Consequently, self-attention probing is not permutation-invariant regarding the frame order, allowing the differentiation of actions with similar appearance but different temporal dynamics.

**Feature Aggregation and Classification.** The embeddings  $\tilde{e}$  are passed through a Multihead Self-Attention (MHSA) layer followed by an average pooling operation:  $p = \frac{1}{T} \sum_{t=1}^T \text{MHSA}(\tilde{e})$ . Unlike prior works [3, 57, 64, 65], we use a pure MHSA block without layer normalization, residual connections, or Feedforward (FF) layers, reducing the parameter count by approximately 3× while maintaining or slightly improving performance. While average pooling itself is permutation-invariant [25], the MHSA embeddings fed into it explicitly encode temporal order through frame-wise positional encodings and interactions with the global CLS token. Thus, the temporal order information is effectively preserved despite pooling (further detailed in the supplementary material). Finally, the pooled representation  $p$  is passed to the linear classification layer.

**4. Experiments**

**4.1. Evaluation setup**

We evaluate STEP using image-pretrained CLIP [42] and DinoV2 [39] foundation models with ViT-B backbones across four diverse action recognition datasets. NTU-RGB+D-120 captures coarse-grained daily activities [30], while IKEA-ASM[6] and Drive&Act[38] focus on fine-grained hand-object assembly and in-car driver behavior, respectively. Something-Something v2 [16] involves complex human-object interactions, requiring an understanding of motion primitives. We adhere to the standard evaluation protocols of prior work, except for our nearly symmetric actions setup. For low-data experiments on SSv2, we randomly sample 5%, 10%, or 25% of each class for training while maintaining class distribution. The full test set is used for evaluation to ensure consistency across models.

**Nearly Symmetric Actions Splits.** To study the impact of sensitivity to temporal order, we also define the concept

of *nearly symmetric actions* as actions with usually similar frame appearance but nearly opposite temporal order. We manually identify such cases at the category level in three datasets rich in such categories – NTU-RGB+D-120, IKEA-ASM and Drive&Act. Examples include *pick up vs. lay down* or *open bottle vs. close bottle* (full split definitions are provided in the supplementary). Our splits result in 20/14/18 (10/7/9 pairs) symmetric and 14/19/102 non-symmetric actions in Drive&Act, IKEA-ASM, and NTU RGB+D 120 respectively.

## 4.2. Comparison to Probing Baselines

We compare our model to three commonly used image-to-video probing methods: 1) linear probing [3, 9, 39] 2) attentive probing [3, 49, 57, 64, 65], which utilizes a cross attention block with a learnable query vector and 3) self-attention probing [35], that has self-attention block with average pooling. Out of these paradigms, attentive probing is presumably the most popular strategy.

Model	NTU-RGB+D 120		Drive&Act	IKEA-ASM	SSv2
	Cross-Sub	Cross-Set			
<b>CLIP</b>					
Linear Probing	57.98	59.5	43.51	34.96	15.18
Attentive Probing	79.76	79.85	64.91	60.7	35.43
Self-Attn Probing	80.9	82.36	64.93	57.44	33.45
STEP (Ours)	<b>85.29</b>	<b>84.94</b>	<b>69.32</b>	<b>62.64</b>	<b>42.43</b>
<b>DinoV2</b>					
Linear Probing	53.8	48.84	47.61	34.81	17.72
Attentive Probing	85.37	84.74	69.22	65.76	41.81
Self-Attn Probing	87.71	87.94	71.16	60.78	43.75
STEP (Ours)	<b>90.82</b>	<b>91.42</b>	<b>78.40</b>	<b>76.28</b>	<b>53.82</b>

Table 1. Comparison of commonly used image-to-video probing mechanisms to our method for CLIP and DinoV2 backbones.

As shown in Table 1, STEP yields the best recognition rates across all datasets and backbones. Next, we discuss the accuracy gains compared to the self-attention probing, as STEP can be viewed as a successor of this approach. On the rather coarse-grained NTU-RGB+D 120, STEP shows moderate gains (+3.11/4.39% DinoV2/CLIP, +3.37/2.58% Cross-Sub/Cross-Set). However, its advantage is more pronounced on fine-grained datasets requiring precise temporal understanding: Drive&Act (+7.24/4.39%), IKEA-ASM (+14.87/5.20%), and SSv2 (+10.03/8.98%).

**Impact of Test-time Frame Order Corruptions.** Since temporal order is generally an important element defining human activities, we would expect a human activity recognition model to show reduced performance if the event sequence is altered at test time. To evaluate this, we test the probing methods on three frame order configurations: correct order, random shuffling, and reverse order (Table 2). Conventional probing methods show no performance change across configurations, which is not surprising as they are inherently permutation invariant (see analysis in Section 3.1). In contrast, STEP exhibits a performance drop

Method	Attentive Probing		Self-Attn Probing		STEP		
	Corr.	Rand./ Rev.	Corr.	Rand./ Rev.	Correct	Random	Reverse
NTU	84.74		87.94		<b>91.42</b>	80.85 ↓	66.31 ↓
Drive&Act	69.22		71.16		<b>78.40</b>	65.26 ↓	59.83 ↓
IKEA-ASM	65.76		60.78		<b>76.28</b>	60.85 ↓	55.19 ↓
SSv2	41.81		43.75		<b>53.78</b>	35.76 ↓	24.03 ↓

Table 2. Performance of attention-based probing and STEP with/without shuffled or reversed frames at test time.

when frames are shuffled, especially in the reverse setup, demonstrating its reliance on sequential dependencies.

## 4.3. Performance on Nearly Symmetric Actions

To investigate the effectiveness of STEP in handling nearly symmetric actions (as defined in Section 4.1), we analyze its performance compared to PEFT-based adaptation methods (ST-Adaptor, AIM, VitaCLIP, M2-CLIP) and other probing mechanisms. STEP outperforms probing frameworks across both symmetric and non-symmetric actions, but the performance gain is more significant for symmetric actions. As shown in Table 3, STEP achieves 74.43% on Drive&Act, 74.46% on IKEA-ASM, and 96.79% on NTU for nearly symmetric actions, surpassing Self-Attentive Probing by +14.86% on Drive&Act and +17.16% on IKEA-ASM. For non-symmetric actions, the improvement is smaller, with STEP achieving 82.05% on Drive&Act and 90.46% on NTU.

Method	Nearly Symmetric Actions			Non-Symmetric Actions		
	D&A	IKEA	NTU	D&A	IKEA	NTU
<b>PEFT Frameworks</b>						
ST-Adaptor [40]	66.85	54.89	96.74	<b>85.99</b>	<b>78.53</b>	<b>92.67</b>
AIM [63]	71.01	56.08	95.87	82.24	68.54	92.28
VitaCLIP [59]	69.19	41.76	96.48	80.17	58.32	88.50
M2-CLIP [56]	71.40	69.46	95.71	85.70	57.27	90.31
<b>Probing Frameworks</b>						
Attn Probing	56.25	65.4	77.74	81.16	65.9	85.97
Self-Attn Probing	59.57	57.30	82.23	81.85	68.01	89.35
STEP (Ours)	<b>74.43</b>	<b>74.46</b>	<b>96.79</b>	82.05	77.15	90.46

Table 3. Performance on nearly symmetric vs. non-symmetric actions across various datasets. STEP excels in symmetric actions, while PEFT methods perform better on non-symmetric actions.

Compared to PEFT methods, STEP consistently outperforms them in nearly symmetric actions, demonstrating superior temporal modeling. While PEFT methods model temporal relationships implicitly through additional layers or learnable prompts, STEP’s explicit enforcement of temporal order provides a decisive advantage in nearly symmetric actions, ensuring clear distinctions between visually similar actions that differ in execution sequence. However, for non-symmetric actions, PEFT methods prove more effective, as their implicit temporal modeling generalizes better to diverse motion patterns.

True Activity Class	Top-1 Acc		Most Common Confusion Class	Confusion	
	Attn.	$\Delta$ ( $\uparrow$ )		Attn.	$\Delta$ ( $\downarrow$ )
closing_bottle	0.17	0.29	opening_bottle	0.60	-0.20
closing_door_inside	0.94	-0.12	opening_door_inside	0.06	0.12
closing_door_outside	0.73	0.27	opening_door_outside	0.27	-0.27
closing_laptop	0.22	0.06	Working on laptop	0.28	-0.06
entering_car	0.94	0.06	exiting_car	0.06	-0.06
exiting_car	1	0.0	-	0.0	0.0
fastening_seat_belt	0.89	0.05	unfastening_seat_belt	0.08	-0.06
fetching_an_object	0.51	0.32	placing_an_object	0.37	-0.29
opening_bottle	0.68	0.08	eating	0.11	0.05
opening_door_inside	0.19	0.56	closing_door_inside	0.56	-0.50
opening_door_outside	0.71	0.29	closing_door_outside	0.29	-0.29
opening_laptop	0.24	-0.12	working on laptop	0.47	-0.24
placing_an_object	0.62	0.18	fetching_an_object	0.22	-0.12
putting_laptop_into_bag	0.14	-0.14	placing_an_object	0.29	0.43
putting_on_jacket	0.33	0.05	taking_off_jacket	0.24	0.10
putting_on_sunglasses	0.84	-0.28	talking_on_phone	0.04	0.20
taking_laptop_from_bag	0.43	0.0	placing_an_object	0.43	-0.10
taking_off_jacket	0.67	-0.27	placing_an_object	0.20	0.27
taking_off_sunglasses	0.22	0.13	putting_on_sunglasses	0.22	-0.04
unfastening_seat_belt	0.5	0.25	fastening_seat_belt	0.25	-0.11

Table 4. Analysis of the individual nearly symmetric actions of the Drive&Act dataset, including accuracy and most common confusions.  $\Delta$  showcases comparison to our STEP probing.

Among PEFT approaches, ST-Adaptor [40] achieves the highest accuracy on non-symmetric actions, leveraging bottleneck adaptors to capture diverse temporal relationships. However, it struggles with symmetric actions, especially on the fine-grained IKEA-ASM dataset, where explicit temporal modeling is crucial to distinguish mirrored sequences. M2-CLIP [56] performs best among PEFT methods on *nearly symmetric actions*, benefiting from its temporal difference module for order sensitivity. While PEFT methods excel on the larger, coarse-grained NTU dataset, their performance drops significantly on the smaller, fine-grained IKEA-ASM dataset, raising concerns about their effectiveness in domain-specific settings with limited data.

We further analyze the performance of STEP on individual *nearly symmetric actions* of the Drive&Act dataset. Table 4 presents their overall accuracy with the attentive probing baseline, the activity class most frequently confused with, and the corresponding confusion rate. Interestingly, we see that the model tends to reliably recognize *one* action in a symmetric pair, while the other is often mapped to its nearly symmetric counterpart. For example, *closing bottle* has a correct recognition rate of only 17% cases and is confused with *opening bottle* in 60% of cases. *Opening bottle* on the other hand is correctly recognized 68% of times. With our approach, identifying *closing bottle* works 29% better and the confusion with *opening bottle* falls by 20%. This pattern is repeated for most of the pairs.

We also perform a similar analysis on the IKEA-ASM dataset, especially with the PEFT methods. As shown in Figure 3, STEP consistently outperforms PEFT methods across nearly all actions, with only a few cases where other methods perform comparably. Despite these exceptions, STEP maintains superior overall performance, particularly

ST-Adaptor	0.14	0.56	0.70	0.15	0.47	0.98	0.42	0.66	0.00
	0.00	0.68	0.48	0.10	0.42	0.88	0.12	0.79	0.00
M2-CLIP	0.00	0.60	0.67	0.25	0.75	1.00	0.59	0.67	0.00
Attn. Probe	0.00	0.63	0.61	0.25	0.70	0.73	0.33	0.68	0.00
Self-Attn. Probe	0.00	0.80	0.61	0.85	0.65	0.93	0.67	0.87	1.00
STEP (Ours)	0.00	0.80	0.61	0.85	0.65	0.93	0.67	0.87	1.00

Pick up leg    Pick up table top    Pick up shelf    Pick up side panel    Pick up front panel    Pick up back panel    Lay down leg    Lay down table top    Lay down bottom panel

Figure 3. Class-wise Accuracy comparison of nearly symmetric actions in IKEA-ASM dataset. STEP outperforms PEFT methods and probing baselines, excelling in fine-grained action recognition.

in distinguishing mirror-symmetric actions, reinforcing its advantage in explicit temporal modeling.

#### 4.4. Comparison to State-of-the-Art

In this section, we compare STEP against state-of-the-art models including fully fine-tuned video models as well as the state-of-the-art PEFT methods for image-to-video transfer such as AIM [63], ST-Adaptor [40], VitaCLIP [59] and M2-CLIP [56]. For multimodal methods (VitaCLIP, M2-CLIP), we use only the image encoder, discarding the text branch to ensure a fair comparison.

**IKEA-ASM.** Table 5 compares STEP to state-of-the-art methods on IKEA-ASM, a dataset rich in hand-centric and nearly symmetric actions. STEP achieves 76.28% accuracy, surpassing PEFT methods by  $\sim 5 - 24\%$ , highlighting their limitations on small, domain-specific datasets. Despite its low parameter count, STEP outperforms prior fully-finetuned SOTA methods by  $\sim 4\%$ . Looking at the underlying foundation models, DinoV2 outperforms CLIP, likely due to its self-distillation pretraining on visual features, which captures finer-grained details compared to the image-text pretraining of CLIP.

**Something Something v2.** We now look at the state-of-the-art approaches on the SSv2 dataset in Table 6. MViTv2-L and UniFormer-B achieve the highest performance (73.3% and 71.2%, respectively), likely benefiting from extensive video pre-training. Despite clear improvements compared to attentive probing, STEP falls short compared to PEFT and fully fine-tuned models, which better adapt spatially and temporally to SSv2’s diverse scenes. However, as shown in Table 7, STEP outperforms PEFT methods in low-data settings (5% and 10%), demonstrating its superior data efficiency. This highlights a fundamental limitation of PEFT

Method	Pretrain	Tunable Param(M)	Top-1 Acc.
<b>Methods with full fine-tuning</b>			
I3D [8]	IN-21K	20.4	52.16
ST-GCN (Skeleton) [61]	IN-21K	2.6	66.29
SWIN_v2(Skeleton)	IN-21K	53.4	72.6
<b>Methods with frozen backbone</b>			
AIM (ViT-B/16)	CLIP	11	64.50
ST-Adaptor (ViT-B/16)	CLIP	7.1	70.85
VitaCLIP (ViT-B/16)	CLIP	28.6	52.94
M2-CLIP (ViT-B/16)	CLIP	14.8	65.5
Attentive Probing (ViT-B/16)	CLIP	7.3	60.7
Attentive Probing (ViT-B/14)	DinoV2	7.3	65.76
STEP (ViT-B/16)	CLIP	2.6	62.64
STEP (ViT-B/14)	DinoV2	2.6	<b>76.28</b>

Table 5. Comparison to fully fine-tuned and frozen backbone methods on IKEA-ASM. All models are evaluated on 16 x 3 x 1 views. Views = #frames x #temporal x #spatial

Method	Pretrain	Tunable Param (M)	Top-1 Acc.	Views
<b>Methods with full fine-tuning</b>				
TimeSformer-L[7]	IN-21K	121	62.4	64x1x3
VideoSwin-B[33]	IN-21K	88	69.6	32x1x1
MTV-B[62]	IN-21K	310	67.6	32x4x3
UniFomer-B[26]	K600	50	71.2	32x1x3
MViTv2-L[28]	K400	213	<b>73.3</b>	32x1x3
EVL ViT-B/16[29]	CLIP	86	62.4	32x1x3
<b>Methods with frozen backbone</b>				
AIM (ViT-B/16)[63]	CLIP	14.4	69.1	32x1x3
ST-Adaptor (ViT-B/16)	CLIP	14.3	69.5	32x1x3
VitaCLIP (ViT-B/16)	CLIP	28.7	48.70	-
M2-CLIP (ViT-B/16)	CLIP	29	69.1	32x1x3
Attentive Probing (ViT-B/16)	CLIP	7.3	35.43	32x1x3
Attentive Probing (ViT-B/14)	DinoV2	7.3	41.81	32x1x3
STEP (ViT-B/16)	CLIP	2.6	42.43	32x1x3
STEP (ViT-B/14)	DinoV2	2.6	53.82	32x1x3

Table 6. Comparison to fully fine-tuned and frozen backbone methods on the Something Something v2 (SSv2) dataset.

models: their dependence on large-scale training for strong performance. Our results consistently show that **PEFT struggles in data-limited settings**, whether in naturally small datasets like IKEA-ASM or artificially constrained low-data regimes like SSv2. In contrast, STEP remains robust even with limited supervision, reinforcing its effectiveness for data-efficient image-to-video adaptation.

**Drive&Act.** We now consider the Drive&Act for fine-grained driver activity recognition. Similar to IKEA-ASM, the dataset has a high amount of fine-grained *nearly symmetric actions* – conditions under which STEP is especially powerful. This is reflected in strong results, as our lightweight approach surpasses the best performing fully fine-tuned models TransDARC and UniformerV2 by 1.8%. Our method also achieves a significant improvement over the PEFT methods, surpassing it by  $\sim 0.1 - 4\%$ . These results underscore the effectiveness of STEP probing on fine-

Method	Tunable Param (M)	SSv2 Top-1 Acc			
		5%	10%	25%	100%
ST-Adaptor	14.3	29.6	38.27	<b>47.82</b>	<b>69.3</b>
AIM	14.3	18.79	20.23	34.01	68.10
VitaCLIP	28.7	22.22	35.03	42.46	48.70
M2-CLIP	29	26.84	35.29	47.21	69.10
STEP (Ours)	2.6	<b>33.98</b>	<b>41.60</b>	47.49	53.82

Table 7. SSv2 performance across data regimes. STEP outperforms PEFT methods in low-data settings (5% and 10%), while PEFT methods rely on larger datasets for strong performance.

Method	Pretrain	Tunable Param (M)	Top-1 Acc.
<b>Methods with full fine-tuning</b>			
TransDARC [41]	IN-21K	88	76.17
Uniformerv2 [27]	IN-21K	115	76.71
VideoSwin-B [33]	K400	88	72.88
<b>Methods with frozen backbone</b>			
AIM (ViT-B/16) [63]	CLIP	14.4	76.85
ST-Adaptor (ViT-B/16)	CLIP	7.1	76.81
VitaCLIP (ViT-B/16)	CLIP	28.6	74.91
M2-CLIP (ViT-B/16)	CLIP	14.8	78.32
Attentive Probing (ViT-B/16)	CLIP	7.3	64.91
Attentive Probing (ViT-B/14)	DinoV2	7.3	69.22
STEP (ViT-B/16)	CLIP	2.6	69.32
STEP (ViT-B/14)	DinoV2	2.6	<b>78.40</b>

Table 8. Comparison to fully fine-tuned and frozen backbone methods on the Drive&Act dataset (RGB modality).

grained tasks where temporal order is an important discriminative feature, even with minimal computational overhead. **NTU-RGB+D 120.** Table 12 summarizes the state-of-the-art comparison on NTU-RGB+D 120. Compared to other datasets we use, this benchmark comprises rather coarse daily activities. Compared to the fully-fined methods, we attain stronger results, surpassing ViewCon on both splits and achieve higher accuracy than DVANet in the cross-subject split. With symmetric actions making up only  $\sim 15\%$  of the dataset, PEFT methods perform robustly, even surpassing fully fine-tuned approaches. Notably, ST-Adaptor and AIM demonstrate strong performance in this setting, highlighting the effectiveness of adaptor based PEFT when fine-grained temporal modeling is less critical.

#### 4.5. Ablation Studies

**Impact of Simplified Attention block.** Empirical results show that removing feedforward layers, layer normalization, and residual connections in our single-layer attention block improves efficiency without loss in accuracy, as these components primarily aid deeper networks. We validate this by comparing three self-attention variants: (1) the standard transformer block [53], (2) a variant without the FF layer, and (3) our fully simplified block with only multi-head attention. Table 9 shows that our simplified attention block

Method	NTU	D&A	IKEA
FF + LN + Skip (Block)	89.64	77.27	73.72
LN + Skip (No FF)	89.63	76.55	74.88
Ours (only Attn. layer)	<b>91.42</b>	<b>78.40</b>	<b>76.28</b>

Table 9. Comparison of attention block variants highlighting performance gains.

Method	NTU	D&A	IKEA
Only Global CLS	90.68	70.19	54.11
Only Patch Tokens	90.25	77.29	73.49
Combined (STEP)	<b>91.42</b>	<b>78.40</b>	<b>76.28</b>

Table 10. Ablation of CLS Token vs. Patch Tokens.

Method	NTU	D&A	IKEA
Fixed PE	91.48	76.76	69.53
Hybrid PE	91.17	77.78	74.88
Learnable PE (Ours)	<b>91.42</b>	<b>78.40</b>	<b>76.28</b>

Table 11. Ablation of different positional encoding (PE) types.

Method	Pretrain	Tunable Param (M)	Cross Setup	Cross Subject
<b>Methods with full fine-tuning</b>				
DVNet[47]	K400	-	91.6	90.4
ViewCon[44]	K400	-	87.5	85.6
<b>Methods with frozen backbone</b>				
AIM (ViT-B/16)[63]	CLIP	11	92.97	90.89
ST-Adaptor (ViT-B/16)	CLIP	7.1	<b>93.44</b>	<b>92.86</b>
VitaCLIP (ViT-B/16)	CLIP	28.6	90.06	87.37
M2-CLIP (ViT-B/16)	CLIP	14.8	91.13	91.73
Attentive Probing (ViT-B/16)	CLIP	7.3	79.85	79.76
Attentive Probing (ViT-B/14)	DinoV2	7.3	85.37	84.74
STEP (ViT-B/16)	CLIP	2.6	84.94	85.29
STEP (ViT-B/14)	DinoV2	2.6	91.42	90.81

Table 12. Comparison to fully fine-tuned and frozen backbone methods on the NTU-RGB+D-120 dataset in cross-setup and cross-subject splits. All models are evaluated on 16 x 1 x 1 views.

improves performance while reducing complexity, achieving 91.42% on NTU (+1.78%), 78.40% on Drive&Act (+1.13%), and 76.28% on IKEA-ASM (+1.93%). These results confirm that removing FF layers, layer normalization, and residual connections in the probing layer enhances efficiency, stability, and performance (Refer to Supplemental).

**Impact of Global CLS Token and Frame-wise Temporal Positional Encoding.** We analyze the contributions of individual components in STEP by evaluating the Global CLS Token and Frame-wise Temporal Positional Encoding (PE). Table 13 shows that adding the Global CLS Token provides consistent improvements, with the largest +8% gain on IKEA-ASM, where capturing global context is critical. The Frame-wise Temporal PE further boosts accuracy, particularly on Drive&Act (+5.91%) and IKEA-ASM (+10.78%), reinforcing its importance for nearly symmetric actions. As shown in Table 10, STEP captures both local and global representations by averaging frame-wise patch embeddings, while relying on a Global CLS Token for high-level abstraction. Unlike deeper transformers that depend on a single CLS token, a single-layer probe struggles with fine-grained actions. Our results confirm that Global CLS alone works well for NTU, but underperforms on IKEA-ASM, highlighting the need for patch embeddings to enhance fine-grained recognition. Combining both elements (STEP) yields the highest performance across all datasets.

**Impact of Different Positional Encoding Schemes.** Table 11 studies our probing framework equipped with different positional encoding (PE) for DinoV2. The Learnable

Method	NTU	Drive&Act	IKEA-ASM
<b>Global CLS Token</b>			
Self-Attn. Probing	87.71	71.16	60.78
Self-Attn. Probing w Global CLS	88.08	72.00	68.76
<b>Frame-wise Temporal PE</b>			
Self-Attn. Probing w Temporal PE	89.74	77.07	71.56
STEP	<b>91.42</b>	<b>78.40</b>	<b>76.28</b>

Table 13. Ablation of individual components and their comparison to native self-attention probing without our modifications.

Method	NTU	D&A	IKEA-ASM
Token-wise PE	89.28	73.21 (63.74)	68.37 (59.90)
Frame-wise PE (STEP)	<b>91.31</b>	<b>78.40 (73.80)</b>	<b>76.28(74.46)</b>

Table 14. Ablation of token vs. frame-wise PE. STEP excels especially on nearly symmetric actions (in parentheses).

PE method (used in our STEP approach) has clear benefits compared to the Fixed and Hybrid positional encoding, with the highest differences observed on IKEA-ASM (> 5% difference between the fixed- and learnable configurations). We further compare our frame-wise PE approach with conventional token-wise PE (Table 14), where each token has a unique PE. Despite using half the parameters, we outperform token-wise PE, particularly in *nearly symmetric action* accuracy (values in parentheses), demonstrating its effectiveness in capturing temporal order.

## 5. Conclusion

We studied parameter-efficient image-to-video probing, focusing on *nearly symmetric actions*—visually similar actions unfolding in reverse order. Existing approaches struggle with such actions as they ignore frame order due to permutation-invariant attention. To address this, we proposed STEP, introducing simple yet effective modifications to self-attention probing, improving temporal sensitivity. Across four benchmarks, STEP achieves new state-of-the-art performance on IKEA-ASM and Drive&Act datasets and outperforms probing and PEFT methods on nearly symmetric actions, while using only a third of the learnable parameters. It also surpasses PEFT in data-scarce settings, demonstrating superior data efficiency. However, its lack of spatial adaptation impacts performance in datasets where appearance and motion cues dominate, suggesting future work on lightweight spatial adaptation within STEP.

## References

- [1] Shahzad Ahmad, Sukalpa Chanda, and Yogesh S Rawat. Ez-clip: Efficient zeroshot video action recognition, 2024. 1
- [2] Bang An, Sicheng Zhu, Michael-Andrei Panaitescu-Liess, Chaithanya Kumar Mummadi, and Furong Huang. Perceptionclip: Visual classification by inferring and conditioning on contexts, 2024. 2
- [3] Adrien Bardes, Quentin Garrido, Jean Ponce, Michael Rabat, Yann LeCun, Mahmoud Assran, and Nicolas Ballas. Revisiting feature prediction for learning visual representations from video. *arXiv:2404.08471*, 2024. 2, 3, 4, 5
- [4] Merve Rabia Barın, Görkay Aydemir, and Fatma Güney. Robust bird’s eye view segmentation by adapting dinov2, 2024. 2
- [5] Yonatan Belinkov. Probing classifiers: Promises, shortcomings, and advances, 2021. 4
- [6] Yizhak Ben-Shabat, Xin Yu, Fatemeh Saleh, Dylan Campbell, Cristian Rodriguez-Opazo, Hongdong Li, and Stephen Gould. The ikea asm dataset: Understanding people assembling furniture through actions, objects and pose. In *Proceedings of the IEEE/CVF Winter Conference on Applications of Computer Vision*, pages 847–859, 2021. 2, 4, 6
- [7] Gedas Bertasius, Heng Wang, and Lorenzo Torresani. Is space-time attention all you need for video understanding?, 2021. 7
- [8] Joao Carreira and Andrew Zisserman. Quo vadis, action recognition? A new model and the kinetics dataset. In *CVPR*, 2017. 7
- [9] Ting Chen, Simon Kornblith, Mohammad Norouzi, and Geoffrey Hinton. A simple framework for contrastive learning of visual representations, 2020. 2, 3, 5
- [10] Qin Cheng, Jun Cheng, Zhen Liu, Ziliang Ren, and Jianming Liu. A dense-sparse complementary network for human action recognition based on rgb and skeleton modalities. *Expert Syst. Appl.*, 244(C), 2024. 1
- [11] Tianheng Cheng, Lin Song, Yixiao Ge, Wenyu Liu, Xingang Wang, and Ying Shan. Yolo-world: Real-time open-vocabulary object detection, 2024. 1
- [12] Ekin D. Cubuk, Barret Zoph, Jonathon Shlens, and Quoc V. Le. Randaugment: Practical automated data augmentation with a reduced search space, 2019. 2
- [13] Srijan Das, Saurav Sharma, Rui Dai, Francois Bremond, and Monique Thonnat. Vpn: Learning video-pose embedding for activities of daily living, 2020. 1
- [14] Jacob Devlin, Ming-Wei Chang, Kenton Lee, and Kristina Toutanova. Bert: Pre-training of deep bidirectional transformers for language understanding, 2019. 3
- [15] Alexey Dosovitskiy et al. An image is worth 16x16 words: Transformers for image recognition at scale. In *ICLR*, 2021. 4
- [16] Raghav Goyal, Samira Ebrahimi Kahou, Vincent Michalski, Joanna Materzyńska, Susanne Westphal, Heuna Kim, Valentin Haenel, Ingo Fruend, Peter Yianilos, Moritz Mueller-Freitag, Florian Hoppe, Christian Thureau, Ingo Bax, and Roland Memisevic. The ”something something” video database for learning and evaluating visual common sense, 2017. 2, 4
- [17] Kaiming He, Xinlei Chen, Saining Xie, Yanghao Li, Piotr Dollár, and Ross Girshick. Masked autoencoders are scalable vision learners, 2021. 2
- [18] Joana Palés Huix, Adithya Raju Ganeshan, Johan Fredin Haslum, Magnus Söderberg, Christos Matsoukas, and Kevin Smith. Are natural domain foundation models useful for medical image classification?, 2023. 2
- [19] Dieuwke Hupkes, Sara Veldhoen, and Willem Zuidema. Visualisation and ’diagnostic classifiers’ reveal how recurrent and recursive neural networks process hierarchical structure, 2018. 4
- [20] Ke Jin and Wankou Yang. Clip for lightweight semantic segmentation, 2023. 2
- [21] Chen Ju, Tengda Han, Kunhao Zheng, Ya Zhang, and Weidi Xie. Prompting visual-language models for efficient video understanding, 2022. 2
- [22] Will Kay, Joao Carreira, Karen Simonyan, Brian Zhang, Chloe Hillier, Sudheendra Vijayanarasimhan, Fabio Viola, Tim Green, Trevor Back, Paul Natssev, Mustafa Suleyman, and Andrew Zisserman. The kinetics human action video dataset, 2017. 2
- [23] Alexander Kolesnikov, Xiaohua Zhai, and Lucas Beyer. Revisiting self-supervised visual representation learning, 2019. 2, 3
- [24] Pulkit Kumar, Namitha Padmanabhan, Luke Luo, Sai Saketh Rambhatla, and Abhinav Shrivastava. Trajectory-aligned space-time tokens for few-shot action recognition, 2024. 1
- [25] Juho Lee, Yoonho Lee, Jungtaek Kim, Adam R. Kosiorek, Seungjin Choi, and Yee Whye Teh. Set transformer: A framework for attention-based permutation-invariant neural networks, 2019. 2, 3, 4
- [26] Kunchang Li, Yali Wang, Peng Gao, Guanglu Song, Yu Liu, Hongsheng Li, and Yu Qiao. Uniformer: Unified transformer for efficient spatiotemporal representation learning, 2022. 7
- [27] Kunchang Li, Yali Wang, Yanan He, Yizhuo Li, Yi Wang, Limin Wang, and Yu Qiao. Uniformerv2: Spatiotemporal learning by arming image vits with video uniformer, 2022. 7
- [28] Yanghao Li, Chao-Yuan Wu, Haoqi Fan, Karttikeya Mangalam, Bo Xiong, Jitendra Malik, and Christoph Feichtenhofer. Mvitv2: Improved multiscale vision transformers for classification and detection, 2022. 7
- [29] Ziyi Lin, Shijie Geng, Renrui Zhang, Peng Gao, Gerard de Melo, Xiaogang Wang, Jifeng Dai, Yu Qiao, and Hongsheng Li. Frozen clip models are efficient video learners, 2022. 1, 3, 7
- [30] Jun Liu, Amir Shahroudy, Mauricio Perez, Gang Wang, Ling-Yu Duan, and Alex C Kot. Ntu rgb+ d 120: A large-scale benchmark for 3d human activity understanding. *TPAMI*, 2019. 2, 4, 1
- [31] Mushui Liu, Bozheng Li, and Yunlong Yu. Omniclip: Adapting clip for video recognition with spatial-temporal omni-scale feature learning. *arXiv preprint arXiv:2408.06158*, 2024. 2
- [32] Ruyang Liu, Jingjia Huang, Ge Li, Jiashi Feng, Xinglong Wu, and Thomas H. Li. Revisiting temporal modeling for clip-based image-to-video knowledge transferring, 2023. 3

- [33] Ze Liu, Jia Ning, Yue Cao, Yixuan Wei, Zheng Zhang, Stephen Lin, and Han Hu. Video swin transformer. In *Proceedings of the IEEE/CVF conference on computer vision and pattern recognition*, pages 3202–3211, 2022. 7, 2
- [34] Ze Liu et al. Video swin transformer. *arXiv preprint arXiv:2106.13230*, 2021. 3
- [35] Huaishao Luo, Lei Ji, Ming Zhong, Yang Chen, Wen Lei, Nan Duan, and Tianrui Li. Clip4clip: An empirical study of clip for end to end video clip retrieval, 2021. 3, 4, 5
- [36] Christian Lülfi, Denis Mayr Lima Martins, Marcos Antonio Vaz Salles, Yongluan Zhou, and Fabian Gieseke. Clip-branches: Interactive fine-tuning for text-image retrieval, 2024. 2
- [37] Yiwei Ma, Guohai Xu, Xiaoshuai Sun, Ming Yan, Ji Zhang, and Rongrong Ji. X-clip: End-to-end multi-grained contrastive learning for video-text retrieval. In *ACMMM*, 2022. 3
- [38] Manuel Martin, Alina Roitberg, Monica Haurilet, Matthias Horne, Simon Reiß, Michael Voit, and Rainer Stiefelwagen. Drive&act: A multi-modal dataset for fine-grained driver behavior recognition in autonomous vehicles. In *Proceedings of the IEEE/CVF International Conference on Computer Vision*, pages 2801–2810, 2019. 2, 4, 1
- [39] Maxime Oquab, Timothée Darcet, Théo Moutakanni, Huy Vo, Marc Szafraniec, Vasil Khalidov, Pierre Fernandez, Daniel Haziza, Francisco Massa, Alaaeldin El-Nouby, Mahmoud Assran, Nicolas Ballas, Wojciech Galuba, Russell Howes, Po-Yao Huang, Shang-Wen Li, Ishan Misra, Michael Rabbat, Vasu Sharma, Gabriel Synnaeve, Hu Xu, Hervé Jegou, Julien Mairal, Patrick Labatut, Armand Joulin, and Piotr Bojanowski. Dinov2: Learning robust visual features without supervision, 2024. 1, 2, 3, 4, 5
- [40] Junting Pan, Ziyi Lin, Xiatian Zhu, Jing Shao, and Hongsheng Li. St-adapter: Parameter-efficient image-to-video transfer learning, 2022. 1, 2, 3, 5, 6
- [41] Kunyu Peng, Alina Roitberg, Kailun Yang, Jiaming Zhang, and Rainer Stiefelwagen. Transdarc: Transformer-based driver activity recognition with latent space feature calibration. In *IROS*, 2022. 7
- [42] Alec Radford, Jong Wook Kim, Chris Hallacy, Aditya Ramesh, Gabriel Goh, Sandhini Agarwal, Girish Sastry, Amanda Askell, Pamela Mishkin, Jack Clark, Gretchen Krueger, and Ilya Sutskever. Learning transferable visual models from natural language supervision, 2021. 1, 2, 3, 4
- [43] Konstantin Schall, Kai Uwe Barthel, Nico Hezel, and Klaus Jung. Optimizing clip models for image retrieval with maintained joint-embedding alignment, 2024. 2
- [44] Ketul Shah, Anshul Shah, Chun Pong Lau, Celso M. de Melo, and Rama Chellapp. Multi-view action recognition using contrastive learning. In *2023 IEEE/CVF Winter Conference on Applications of Computer Vision (WACV)*, pages 3370–3380, 2023. 8
- [45] Peter Shaw, Jakob Uszkoreit, and Ashish Vaswani. Self-attention with relative position representations, 2018. 3
- [46] Michal Shlapentokh-Rothman, Ansel Blume, Yao Xiao, Yuqun Wu, Sethuraman T V au2, Heyi Tao, Jae Yong Lee, Wilfredo Torres, Yu-Xiong Wang, and Derek Hoiem. Region-based representations revisited, 2024. 1
- [47] Nyle Siddiqui, Praveen Tirupattur, and Mubarak Shah. Dvanet: Disentangling view and action features for multi-view action recognition, 2023. 8
- [48] Amanpreet Singh, Ronghang Hu, Vedanuj Goswami, Guillaume Couairon, Wojciech Galuba, Marcus Rohrbach, and Douwe Kiela. Flava: A foundational language and vision alignment model, 2022. 2
- [49] Zhan Tong, Yibing Song, Jue Wang, and Limin Wang. Videomae: Masked autoencoders are data-efficient learners for self-supervised video pre-training. *NeurIPS*, 2022. 2, 3, 5, 4
- [50] Shuyuan Tu, Qi Dai, Zuxuan Wu, Zhi-Qi Cheng, Han Hu, and Yu-Gang Jiang. Implicit temporal modeling with learnable alignment for video recognition, 2023. 3
- [51] Narek Tumanyan, Assaf Singer, Shai Bagon, and Tali Dekel. Dino-tracker: Taming dino for self-supervised point tracking in a single video, 2024. 1
- [52] Aaron van den Oord, Yazhe Li, and Oriol Vinyals. Representation learning with contrastive predictive coding, 2019. 2, 3
- [53] Ashish Vaswani et al. Attention is all you need. In *NeurIPS*, 2017. 3, 7, 4
- [54] Mengmeng Wang, Jiazheng Xing, and Yong Liu. Actionclip: A new paradigm for video action recognition, 2021. 2, 3
- [55] Mengmeng Wang, Jiazheng Xing, Boyuan Jiang, Jun Chen, Jianbiao Mei, Xingxing Zuo, Guang Dai, Jingdong Wang, and Yong Liu. M2-clip: A multimodal, multi-task adapting framework for video action recognition, 2024. 1
- [56] Mengmeng Wang, Jiazheng Xing, Boyuan Jiang, Jun Chen, Jianbiao Mei, Xingxing Zuo, Guang Dai, Jingdong Wang, and Yong Liu. M2-clip: A multimodal, multi-task adapting framework for video action recognition. *arXiv preprint arXiv:2401.11649*, 2024. 2, 3, 5, 6
- [57] Yi Wang, Kunchang Li, Xinhao Li, Jiashuo Yu, Yinan He, Chenting Wang, Guo Chen, Baoqi Pei, Ziang Yan, Rongkun Zheng, Jilan Xu, Zun Wang, Yansong Shi, Tianxiang Jiang, Songze Li, Hongjie Zhang, Yifei Huang, Yu Qiao, Yali Wang, and Limin Wang. Internvideo2: Scaling foundation models for multimodal video understanding, 2024. 2, 3, 4, 5
- [58] Yuan Wang, Rui Sun, Naisong Luo, Yuwen Pan, and Tianzhu Zhang. Image-to-image matching via foundation models: A new perspective for open-vocabulary semantic segmentation, 2024. 2
- [59] Syed Talal Wasim, Muzammal Naseer, Salman Khan, Fahad Shahbaz Khan, and Mubarak Shah. Vita-clip: Video and text adaptive clip via multimodal prompting. In *Proceedings of the IEEE/CVF Conference on Computer Vision and Pattern Recognition*, pages 23034–23044, 2023. 2, 3, 5, 6
- [60] Wenhao Wu, Xiaohan Wang, Haipeng Luo, Jingdong Wang, Yi Yang, and Wanli Ouyang. Bidirectional cross-modal knowledge exploration for video recognition with pre-trained vision-language models, 2023. 3
- [61] Sijie Yan, Yuanjun Xiong, and Dahua Lin. Spatial temporal graph convolutional networks for skeleton-based action recognition, 2018. 7
- [62] Shen Yan, Xuehan Xiong, Anurag Arnab, Zhichao Lu, Mi Zhang, Chen Sun, and Cordelia Schmid. Multiview transformers for video recognition, 2022. 7

- [63] Taojiannan Yang, Yi Zhu, Yusheng Xie, Aston Zhang, Chen Chen, and Mu Li. Aim: Adapting image models for efficient video action recognition, 2023. [1](#), [2](#), [3](#), [5](#), [6](#), [7](#), [8](#)
- [64] Jiahui Yu, Zirui Wang, Vijay Vasudevan, Legg Yeung, Mojtaba Seyedhosseini, and Yonghui Wu. Coca: Contrastive captioners are image-text foundation models, 2022. [2](#), [4](#), [5](#), [3](#)
- [65] Liangzhe Yuan, Nitesh Bharadwaj Gundavarapu, Long Zhao, Hao Zhou, Yin Cui, Lu Jiang, Xuan Yang, Menglin Jia, Tobias Weyand, Luke Friedman, Mikhail Sirotenko, Huisheng Wang, Florian Schroff, Hartwig Adam, Ming-Hsuan Yang, Ting Liu, and Boqing Gong. Videoglue: Video general understanding evaluation of foundation models, 2024. [2](#), [4](#), [5](#), [3](#)
- [66] Luca Zanella, Benedetta Liberatori, Willi Menapace, Fabio Poiesi, Yiming Wang, and Elisa Ricci. Delving into clip latent space for video anomaly recognition, 2023. [1](#)
- [67] Zhun Zhong, Liang Zheng, Guoliang Kang, Shaozi Li, and Yi Yang. Random erasing data augmentation, 2017. [2](#)

# Order Matters: On Parameter-Efficient Image-to-Video Probing for Recognizing Nearly Symmetric Actions

## Supplementary Material

### A. Nearly Symmetric Action Splits.

In Tables 15, 16 and 17 we provide the full list of the newly defined nearly symmetric actions pairs in the Drive&Act, IKEA-ASM, and NTU-RGB+D 120 datasets respectively. All categories not listed in these tables are regarded as non-symmetric. The resulting splits include 20/14/18 actions (10/7/9 pairs) classified as symmetric and 14/19/108 actions as non-symmetric in Drive&Act, IKEA-ASM, and NTU-RGB+D 120 respectively.

Action Type	Action	Counterpart
<b>Opening/Closing</b>	Closing Bottle	Opening Bottle
	Closing Door (Inside)	Opening Door (Inside)
	Closing Door (Outside)	Opening Door (Outside)
	Closing Laptop	Opening Laptop
<b>Entering/Exiting</b>	Entering Car	Exiting Car
<b>Fastening/Unfastening</b>	Fastening Seat Belt	Unfastening Seat Belt
<b>Fetching/Placing</b>	Fetching an Object	Placing an Object
<b>Putting/Taking</b>	Putting Laptop into Backpack	Taking Laptop from Backpack
	Putting on Jacket	Taking off Jacket
	Putting on Sunglasses	Taking off Sunglasses

Table 15. An overview of the defined nearly symmetric action pairs on the Drive&Act Dataset.

Action Type	Action	Counterpart
<b>Picking/Laying</b>	Pick Up Leg	Lay Down Leg
	Pick Up Table Top	Lay Down Table Top
	Pick Up Shelf	Lay Down Shelf
	Pick Up Side Panel	Lay Down Side Panel
	Pick Up Front Panel	Lay Down Front Panel
	Pick Up Back Panel	Lay Down Back Panel
	Pick Up Bottom Panel	Lay Down Bottom Panel

Table 16. An overview of the defined nearly symmetric action pairs on the IKEA-ASM Dataset.

Action Type	Action	Counterpart
<b>Sitting/Standing</b>	Sit Down	Stand Up
<b>Putting On/Taking Off</b>	Put on Jacket	Take off Jacket
	Put on a Shoe	Take off a Shoe
	Put on Glasses	Take off Glasses
	Put on a Hat/Cap	Take off a Hat/Cap
	Put on Headphone	Take off Headphone
	Put on Bag	Take off Bag
<b>Walking Directions</b>	Walking Towards	Walking Apart
<b>Placing/Retrieving</b>	Put Object into Bag	Take Object out of Bag

Table 17. An overview of the defined nearly symmetric action pairs in the NTU-RGB+D 120 Dataset.

### B. Benchmark and Implementation Details

**NTU-RGB+D 120** [30] is a large-scale benchmark for human activity recognition, featuring 120 action classes performed by 106 subjects across various settings. It includes over 114,000 video samples captured from three fixed camera viewpoints, offering RGB, depth, infrared (IR), and 3D skeleton data. The dataset encompasses various actions, including daily activities, health-related actions, and mutual interactions, making it suitable for evaluating action recognition models. Most existing works on the NTU dataset utilize both RGB and skeleton data [10, 13]; however, we focus exclusively on the RGB modality.

For the NTU dataset, we follow the practice of cropping around the human before inputting data into the model. Unlike existing RGB-only models [13], which rely on human poses for cropping, we utilize an open-vocabulary object detector, YOLO-World [11], with the prompt “human” to generate bounding boxes. A center crop is applied around these bounding boxes. For actions involving two humans, we create a bounding box encompassing both individuals by considering the leftmost and rightmost coordinates.

During training, we freeze the image foundation models and train the probes on 4 NVIDIA A-100 GPUs with a batch size of 32 for 60 epochs. The learning rate is initialized at 1e-3, using the SGD optimizer with a weight decay of 0.02 and a cosine annealing scheduler. Spatial data augmentation is applied to generate 224×224 crops, with basic techniques such as cropping and flipping, yet achieving strong performance. We evaluate the model on the NTU dataset using the cross-subject and cross-setup benchmarks [30]. For testing, we use 16 frames obtained via uniform sampling, dividing each video into 16 sections and randomly sampling one frame per section.

**Drive&Act** [38] is a comprehensive driver activity recognition dataset featuring fine-grained actions captured from 15 drivers (11 male, 4 female) with diverse physical attributes. The dataset provides 34 fine-grained activity labels in a hierarchical structure. It includes RGB, infrared (NIR), depth, and 3D skeleton data from six distinct viewpoints. For our experiments, we use only the RGB modality, as Vision Foundation models like CLIP [42] and DinoV2 [39] are pre-trained exclusively on RGB images.

We further identify symmetric action pairs within the dataset to assess the performance of various probes on these actions. Table 15 outlines the identified symmetric actions, serving as a resource for future research on symmetric action recognition within the Drive&Act dataset.

We follow the basic data preprocessing steps outlined by the authors [38] to ensure a fair evaluation. While we adopt the same augmentations and settings as used for the NTU-RGB+D 120 dataset, we use an AdamW optimizer instead of SGD. For evaluation, we adhere to the protocol provided by the authors [38], which divides the dataset into three splits: ten subjects for training, two for validation, and three for testing. We train separate models for each split and evaluate performance as the average across the three test splits. During testing, 16 frames are sampled with a frame interval of 2, and three clips are sampled along the temporal dimension. Final performance is obtained by ensembling predictions across three views.

**IKEA-ASM** [6] is a comprehensive furniture assembly dataset featuring 371 assembly processes performed by 48 participants across five settings, including offices, labs, and homes. It provides RGB, depth, and 3D skeleton data from three perspectives, totaling 35 hours of footage and covering 33 fine-grained activities. Following the approach used for the Drive&Act dataset, we identify symmetric actions within IKEA-ASM and present an overview of them in Table 16.

We adopt the environment-based split recommended by the authors [6], ensuring no overlap between training and testing environments. We further divide the training set into training and validation subsets to align with our protocols while retaining the original test configuration. Specifically, two environments are used for training, one for validation, and two for testing. We follow the same training regime and augmentations as in the Drive&Act dataset. During testing, 16 frames are sampled with a frame interval of 2, and three clips are sampled along the temporal dimension. The final performance is obtained by ensembling predictions across three views.

**Something Something v2** dataset [16] is a large-scale benchmark designed for fine-grained action recognition with a focus on temporal dynamics. It consists of 220,847 video clips covering 174 action classes. These classes emphasize temporal relationships and object interactions, such as "Pushing something from left to right" or "Moving something closer to the camera." The dataset is particularly challenging due to the high reliance on motion primitives and temporal cues for accurate recognition.

For our experiments, we preprocess the data following the standard protocols outlined by the authors [16]. We incorporate augmentation techniques inspired by [33], along with stronger augmentations such as Random Augmentation [12] and Random Erasing [67], similar to [63]. To enhance training stability, we use the AdamW optimizer.

The dataset is divided into three predefined splits: training (168,913 videos), validation (24,777 videos), and testing (27,157 videos). During testing, we sample three random clips along the spatial axis to account for intra-video

variability. Final predictions are obtained by ensembling the outputs of these sampled clips, ensuring robust and reliable performance.

### C. Permutation Invariance Analysis

The embeddings are first enriched with learnable frame-wise positional encodings (PE) before entering the self-attention mechanism:

$$\tilde{e}_t = e_t + PE(t), \quad t = 1, \dots, T \quad (3)$$

where  $e_t$  is the original frame embedding, and  $PE(t)$  is a learnable encoding that assigns a unique temporal position to each frame. This ensures that each frame contains position-dependent information before undergoing attention-based transformation.

The enriched embeddings  $\tilde{e}$  are then processed by a Multihead Self-Attention (MHSA) layer, followed by an average pooling operation:

$$p = \frac{1}{T} \sum_{t=1}^T \text{MHSA}(\tilde{e}_t) \quad (4)$$

A potential concern arises due to the permutation-invariant nature of average pooling, which treats all frames equally, potentially discarding temporal order. However, since the MHSA operation attends to position-encoded inputs, it outputs temporally aware representations. Thus, although the final aggregation step does not explicitly retain order, it pools embeddings that have already been temporally structured by self-attention.

If PE is applied *after* MHSA instead of before, it is simply added to the pooled output:

$$p' = \left( \frac{1}{T} \sum_{t=1}^T \text{MHSA}(e_t) \right) + PE \quad (5)$$

Since addition is commutative, this operation does not encode sequence-specific dependencies, making the representation permutation-invariant. Empirical validation in Table 18 confirms this: applying PE before MHSA leads to performance drops when frames are shuffled, indicating reliance on temporal structure. In contrast, applying PE after MHSA yields nearly identical results across different frame orders, confirming its ineffectiveness in enforcing temporal sensitivity.

These results highlight that while average pooling itself is permutation-invariant, temporal information is preserved as long as PE is introduced before self-attention. This allows the model to effectively retain sequence awareness while maintaining parameter efficiency.

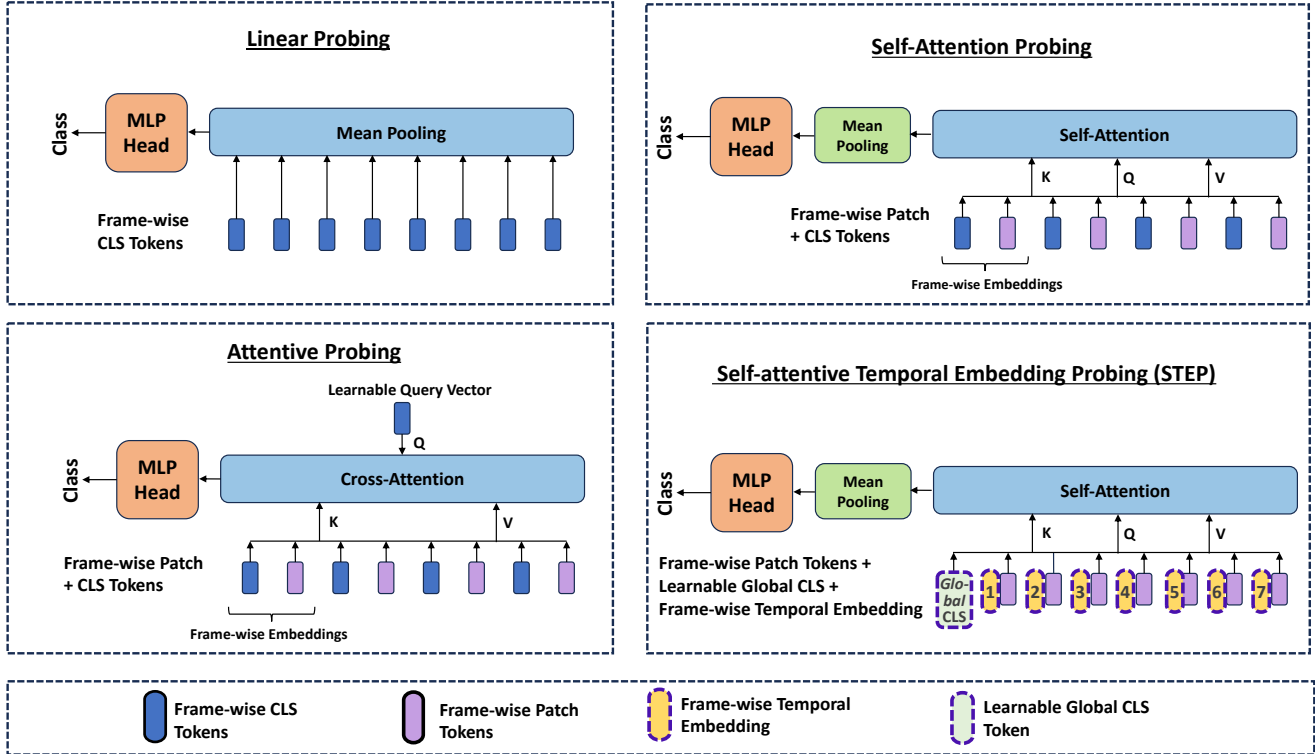


Figure 4. **Overview of Probing Mechanisms for Video Action Recognition.** (Top left) Linear probing uses mean pooling over frame-wise CLS tokens. (Top right) Self-attention probing incorporates frame-wise embeddings with self-attention and mean pooling. (Bottom left) Attentive probing leverages cross-attention with a learnable query. (Bottom right) STEP integrates frame-wise patch tokens, temporal embeddings, and a global CLS token with self-attention for temporal modeling.

Method	Drive&Act		IKEA-ASM	
	Correct	Reverse	Correct	Reverse
STEP w PE AFTER MHSA	70.34	70.34	70.08	70.08
STEP	78.40	59.83	76.28	55.19

Table 18. Performance comparison of STEP with positional encoding applied before vs. after MHSA. Applying PE before MHSA retains order sensitivity, while adding PE after MHSA results in permutation invariance.

#### D. Details on Image-to-Video Probing Mechanisms for Video Action Recognition

Figure 4 illustrates the key difference between our approach and three prominent probing to adapt image foundation models for video action recognition: linear probing [3, 9, 39], attentive probing [3, 49, 57, 64, 65], and self-attentive probing [35]. These approaches differ in their ability to model temporal relationships and utilize frame-wise embeddings.

**Linear Probing:** A baseline method that applies mean pooling over frame-wise CLS tokens, followed by an MLP head. This approach lacks temporal modeling but serves as a simple baseline.

**Self-Attention Probing:** Combines frame-wise patch and CLS tokens with a self-attention mechanism to capture temporal dependencies across frames, enhancing temporal modeling. The resulting features are then aggregated using mean pooling.

**Attentive Probing:** Utilizes a learnable query vector with cross-attention to extract relevant information from frame-wise embeddings, focusing on selective temporal aggregation. This is presumably the most commonly used image-to-video probing strategy [3, 49, 57, 64, 65].

**Self-attentive Temporal Embedding Probing (STEP):** Our STEP approach builds on self-attention by introducing frame-wise temporal embeddings and a learnable global CLS token, enabling efficient temporal modeling across frames while maintaining simplicity.

These mechanisms highlight the trade-offs between simplicity, parameter efficiency, and temporal modeling, with STEP offering an optimal balance for fine-grained video recognition.

#### E. Additional Experiments

**Details on the Simplified Classification Head.** Next, we shed light on the proposed simplification of the classifi-

cation head, leading to a significant decrease in parameters and slightly improving the action recognition results. Baseline attentive probing [3, 49, 57, 64, 65], introduce non-linearity in the probe to extract complex features from the generalized representations from the foundation models. However, complex non-linear probes can “bear the risk that the classifier (probe) infers features that are not actually used by the network (Foundation model)” [5, 19]. To mitigate this, we simplify our attention block by removing layer normalization, residual connections, and Feedforward (FF) projection layers. This design choice offers two key benefits: (1) it reduces the non-linearity of the probe by eliminating the activation function in the FF layers, and (2) it **decreases the number of parameters significantly**, from 7.3M to 2.6M. Although some non-linearity remains due to the softmax activation in attention weights, FF activation functions are the primary contributors to non-linearity in standard attention blocks.

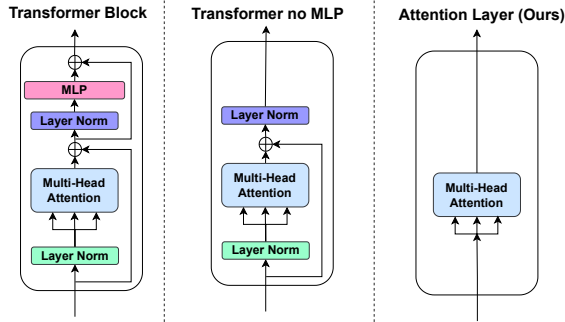


Figure 5. Architectural comparison of standard transformer block, no-FF variant, and the **proposed simplified attention block** used in our STEP framework, highlighting the removal of non-linear components.

Empirical results show that the simplified attention block retains performance and slightly improves it, as the removed components are primarily beneficial for stability in deeper networks. As our probing setup uses only a single attention layer, we find these components to be unnecessary, allowing for efficient learning while maintaining accuracy. To validate our findings, we conduct experiments with three variants of the self-attention block: (1) the standard transformer block from [53], (2) a variant without the FF layer, and (3) our fully simplified block with only multi-head attention. Figure 5 provides an overview of these architectures, and our results demonstrate that the simplified block offers improved performance with reduced complexity.

Table 19 reflects the effectiveness of our simplified attention block across the NTU-RGB+D 120, Drive&Act, and IKEA-ASM datasets. On NTU-RGB+D 120, the proposed design achieves 91.42% accuracy, improving upon the standard transformer block by 1.78%, highlighting the benefits

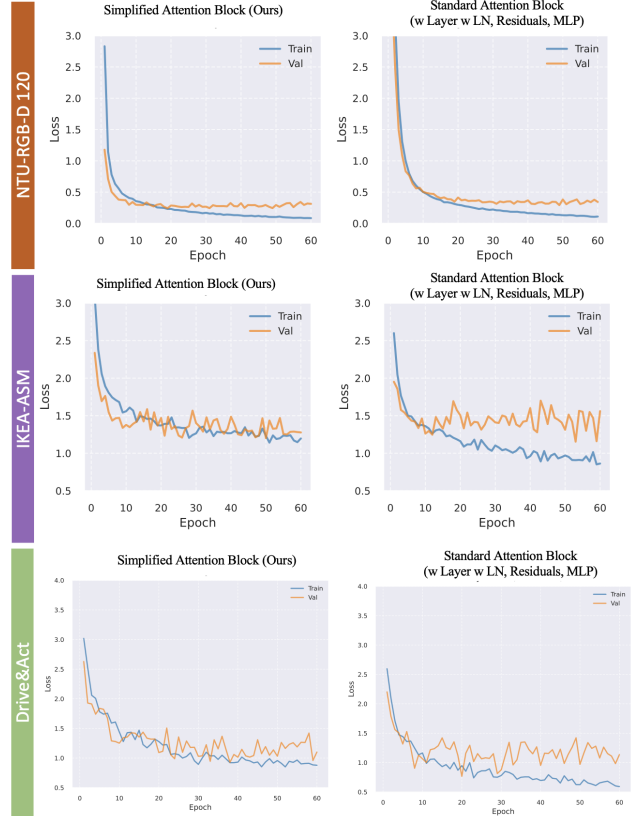


Figure 6. Loss curves comparing Simplified vs. Standard Attention Blocks on NTU-RGB+D 120, IKEA-ASM, and Drive&Act. Our approach shows faster convergence and less overfitting.

Method	Params	NTU	Drive&Act	IKEA-ASM
<b>STEP</b>				
FF+LN+Skip (Block)	7.1	89.64	77.27	73.72
LN+Skip (No MLP)	2.6	89.63	76.55	74.88
Ours (only Attn. layer)	<b>2.6</b>	<b>91.42</b>	<b>78.4</b>	<b>76.28</b>

Table 19. Comparison of attention block variants on NTU, Drive&Act, and IKEA-ASM datasets, showing performance improvements and parameter efficiency of the proposed block.

of reduced complexity while probing coarser actions. Similarly, on Drive&Act, our method achieves 78.4%, surpassing the transformer block by 1.13% and the no-FF variant by 1.85%, showing its ability to capture fine-grained temporal dependencies. For IKEA-ASM, a dataset requiring nuanced temporal modeling, our approach achieves 76.28%, outperforming the full transformer block by 1.93%. Moreover, the training curves shown in Figure 6 highlight faster convergence and reduced overfitting, particularly on IKEA-ASM, where the full transformer block exhibits greater validation loss fluctuations. These results confirm that removing FF layers, layer normalization, and residual connections enhances both efficiency and stability while maintaining strong performance.

**Performance Analysis on Nearly Symmetric and non-Symmetric Actions.** In addition to our analysis of STEP on the nearly symmetric actions. We perform a similar analysis on the non-symmetric actions of the Drive&Act dataset.

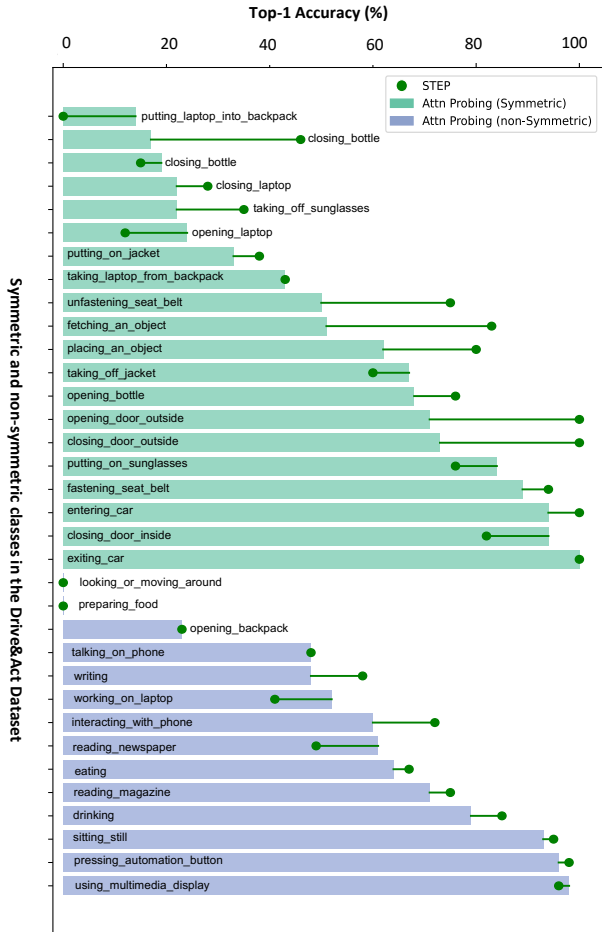


Figure 7. Class-wise comparison of STEP and attentive probing on symmetric and non-symmetric actions in the Drive&Act dataset, showcasing consistent performance improvements with STEP.

Figure 7 provides a detailed class-wise comparison of the improvements achieved by STEP over attentive probing for both nearly symmetric and non-symmetric actions. The results demonstrate that STEP consistently outperforms attentive probing across both categories. For nearly symmetric actions (e.g., *opening bottle* vs. *closing bottle*), the incorporation of temporal embeddings in STEP significantly enhances its ability to capture subtle temporal differences, leading to marked performance gains. Similarly, for non-symmetric actions (e.g., *interacting with phone* or *writing*), STEP shows robust improvements by better modeling the complex temporal dynamics inherent in these actions. This evaluation underscores the universal applicability of STEP, which not only excels in capturing fine-grained

temporal distinctions in nearly symmetric actions but also demonstrates strong generalization to more diverse, non-symmetric activities.

**Impact of Temporal Embedding on Probing mechanisms.** To evaluate the impact of incorporating frame-wise temporal embeddings, we apply our learnable frame-wise temporal positional encoding (PE) to both attentive probing [3, 49, 57, 64] and self-attention probing [35]. Table 20 summarizes the results, demonstrating the universal applicability and performance improvements achieved by adding learnable temporal embeddings.

Method	NTU	Drive&Act	IKEA-ASM
Attentive Probing	<b>84.74</b>	68.22	65.76
Attentive Probing + Learnable PE	82.58	<b>70.04</b>	<b>67.83</b>
Self-Attention Probing	87.94	71.16	60.78
Self-Attention + Learnable PE	<b>91.20</b>	<b>77.07</b>	<b>71.56</b>
STEP	91.42	78.4	76.28

Table 20. Performance comparison of Attentive Probing and Self-Attention Probing with and without learnable temporal PE across NTU, Drive&Act, and IKEA-ASM datasets, highlighting consistent improvements with PE integration.

The inclusion of frame-wise learnable temporal PE in Self-Attention Probing results in significant improvements across all datasets, with gains of +3.26% on NTU, +5.91% on Drive&Act, and +10.78% on the most fine-grained IKEA-ASM, highlighting its effectiveness in capturing temporal dependencies. We achieve smaller gains in attentive probing with improvements in Drive&Act (+1.82%) and IKEA-ASM (+2.07%). These results indicate that learnable frame-wise temporal positional encoding enhances temporal modeling capabilities for both types of probing, benefiting datasets with varying levels of granularity.

**Effect of Frame Count on performance.** Table 21 demonstrates the effect of varying the number of input frames on the performance of the STEP method across NTU, Drive&Act, and IKEA-ASM datasets. As the frame count increases from 4 to 16, there is a consistent improvement in accuracy across all datasets. This highlights the importance of capturing more temporal context for effective action recognition.

The improvement is most notable in the IKEA-ASM dataset, where accuracy increases significantly from 65.04% (4 frames) to 75.65% (16 frames). This dataset contains the most fine-grained actions among the three, making it particularly reliant on detailed temporal modeling. In contrast, datasets like NTU and Drive&Act, which contain relatively coarser or moderately fine-grained actions, exhibit smaller but consistent gains with an increasing number of frames. These results emphasize the critical role of temporal information, especially for datasets with high granularity in action representation.

Method	NTU	Drive&Act	IKEA-ASM
<b>STEP</b>			
4 frames	88.07	74.85	65.04
8 frames	90.60	77.68	71.39
16 frames	<b>91.42</b>	<b>78.40</b>	<b>76.28</b>

Table 21. Performance of STEP on NTU, Drive&Act, and IKEA-ASM with varying frame counts (4, 8, 16). IKEA-ASM, with the most fine-grained actions, shows the largest improvement, highlighting the importance of temporal information in fine-grained HAR.

Method	Tunable Param (M)	Verb Accuracy	Object Accuracy
<b>PEFT Frameworks</b>			
ST-Adaptor	7.1	70.92	75.42
AIM	11	67.24	72.55
VitaCLIP	28.6	52.04	56.84
M2-CLIP	14.8	68.57	71.33
<b>Probing Frameworks</b>			
Attentive Probing	7.3	66.02	70.61
Self-Attn Probing	2.6	70.0	74.20
STEP (Ours)	2.6	<b>79.29</b>	<b>81.02</b>

Table 22. Comparison of verb and object accuracy on IKEA-ASM. STEP outperforms both PEFT and probing methods, highlighting its ability to capture temporal dependencies while maintaining strong object recognition.

**Verb-Object Factorization Analysis in IKEA-ASM.** We analyze verb and object recognition performance in the IKEA-ASM dataset using its verb-object factorization [6]. Table 22 shows that STEP significantly outperforms both probing and PEFT methods across verb and object accuracies. Compared to the best PEFT method (ST-Adaptor), STEP improves verb accuracy by +8.37% and object accuracy by +5.6%. Against attentive probing, it achieves gains of +13.27% and +10.41% in verb and object accuracy respectively.

The design choices in STEP, particularly the use of patch tokens and the global CLS token, enhance spatial representation, leading to strong object recognition accuracy. Notably, while PEFT methods incorporate spatial adaptation, they struggle not only with verb recognition—which relies on temporal understanding—but also with object-level distinctions. This suggests that PEFT methods depend on large-scale training data for effective adaptation. In contrast, STEP achieves superior performance even in a smaller dataset like IKEA-ASM, demonstrating its effectiveness in data-efficient image-to-video transfer.

## F. Qualitative Evaluation

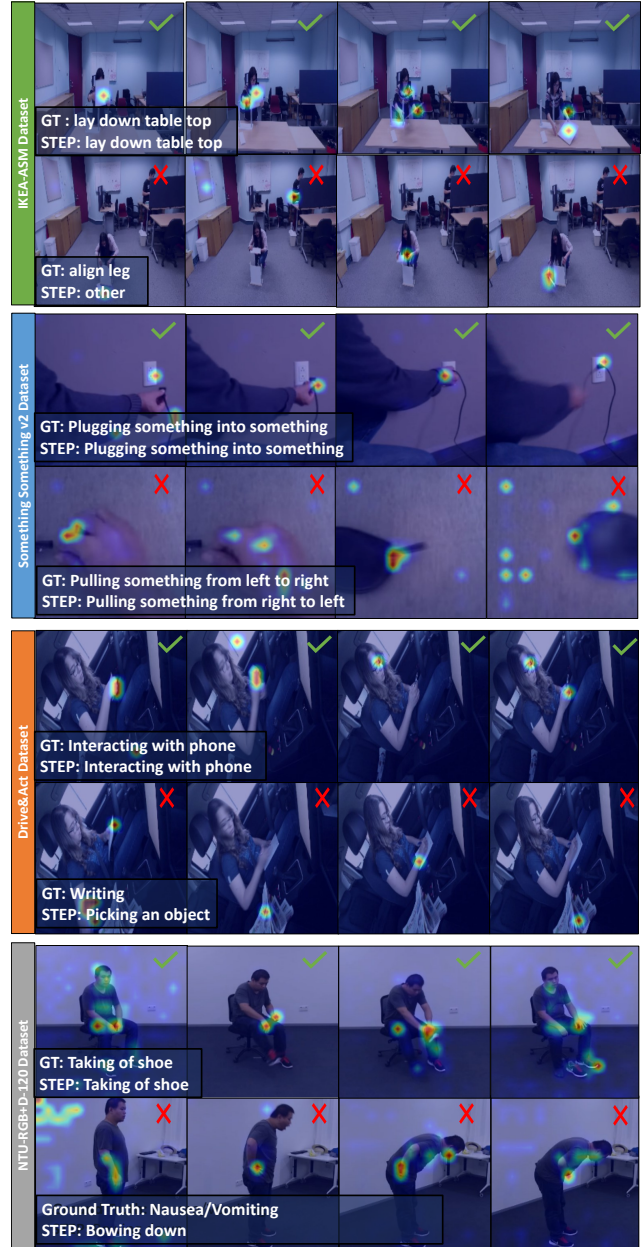


Figure 8. Qualitative results and attention maps of our approach, with examples of correct classifications (✓) and mistakes (✗).

In Figure 8, we revisit the attention maps of the frames for correct and incorrect predictions of our approach. In the fine-grained IKEA-ASM dataset, STEP correctly attends to the human and relevant object (furniture parts). However, the cluttered environment with unrelated objects and people can lead to emphasized background figures, causing misclassification. In the SSv2 dataset examples, STEP identifies key objects and human figures well, focusing on hands and

objects but struggles with spatial reasoning (*pulling something from left to right* recognized as *pulling something from right to left*). In the fine-grained **Drive&Act** dataset, our approach focuses on correct key elements like eyes and hands, but there are sometimes misclassified actions due to background distractions. In the **NTU-RGB+D 120** examples, our method attends to the expected elements like the hands and the shoes when classifying *taking off a shoe*. However, there are rare instances where STEP struggles, often in cases that are challenging even for humans. For example, STEP may misclassify *nausea* as *bowing down*. Despite correctly focusing on the mouth area, the subtle difference between these actions proves difficult for the model, indicating the need for even finer spatial sensitivity in such cases.